Published in final edited form as:
Science. 2006 March 17; 311(5767): 1609–1612. doi:10.1126/science.1121449.

αE-catenin controls cerebral cortical size by regulating hedgehog signalling pathway

Wen-Hui Lien[1,2,4], **Olga Klezovitch**[1,4], **Tania E. Fernandez**[1], **Jeff Delrow**[3], and **Valeri Vasioukhin**[1,*]

1 *Division of Human Biology, Fred Hutchinson Cancer Research Center, Seattle, WA, 98109*

2 *Molecular and Cellular Biology Program, University of Washington, Seattle, WA, 98195*

3 *Genomics Resource, Fred Hutchinson Cancer Research Center, Seattle, WA, 98109*

Abstract

During development cells monitor and adjust their rates of accumulation to produce predetermined-size organs; however, responsible for this mechanisms remain unknown. We show here that central nervous system-specific deletion of the essential adherens junction gene, *αE-catenin*, causes abnormal activation of the hedgehog pathway resulting in shortening of the cell cycle, decreased apoptosis and subsequent massive cortical hyperplasia. We propose that αE-catenin connects cell-density-dependent adherens junctions with the developmental hedgehog pathway and this connection may provide a negative feedback loop controlling the size of developing cerebral cortex.

Keywords

mammalian brain development; hedgehog pathway; neural progenitor cells

During brain development, proliferation of neural progenitor cells is tightly controlled to produce the organ of predetermined size. We hypothesized that cell-cell adhesion structures may be involved in this function because they can provide cells with information concerning the density of their cellular neighborhood. Intercellular adhesion in neural progenitors is mediated primarily by adherens junctions, which contain cadherins, β- and α-catenins (1). We found that progenitors express αE(epithelial)-catenin, while differentiated neurons express αN(neural)-catenin (Fig. S1A–D). Since α-catenin is critical for the formation of adherens junctions (2,3), we decided to determine the role of these adhesion structures in neural progenitor cells by generating mice with CNS-specific deletion of *αE-catenin*. Mice with a conditional *αE-catenin* allele (*αE-catenin*$^{loxP/loxP}$) (4) were crossed with mice carrying nestin-promoter-driven Cre recombinase (*Nestin-Cre*$^{+/-}$), which is expressed in CNS stem/neural progenitors starting at embryonic day E10.5 (5) (Fig. S1E). The resulting *αE-catenin*$^{loxP/loxP}$/*Nestin-Cre*$^{+/-}$ animals displayed loss of αE-catenin in neural progenitor cells and its presence in the blood vessels not targeted by *Nestin-Cre* (Figs. 2D–F, S1F).

While no phenotype was observed in heterozygous *αE-catenin*$^{loxP/+}$/*Nestin-Cre*$^{+/-}$mice, the knockout *αE-catenin*$^{loxP/loxP}$/*Nestin-Cre*$^{+/-}$ mice were born with bodies similar to their littermates, but with enlarged heads (Fig. S2A). After birth, the heads of these animals continued to grow, but their bodies were developmentally-retarded generating abnormal large-

*Correspondence: Valeri Vasioukhin, Ph.D., Division of Human Biology, Fred Hutchinson Cancer Research Center, 1100 Fairview Ave N., C3-168, Seattle, WA 98109, Phone: 206 667 1710, Fax: 206 667 6524, E-mail: vvasiouk@fhcrc.org.
[4]These authors contributed equally

headed pups that failed to thrive and died between 2–3 weeks of age (Fig. S2B). Counting brain cell numbers at different points of embryonic development revealed massive hyperplasia in the mutant brains, with a 2-fold increase in total brain cell numbers by the time of birth (Fig. S2C). While no differences were found at E12.5, mutant brains displayed a 40% increase in total cell numbers only one day later at E13.5. In addition to an increase in brain cell numbers, the mutant animals displayed increases in brain weights and brain-to-bodyweight ratios (Fig. S2D, E). Histologic analysis of *αE-catenin*$^{loxP/loxP}$*/Nestin-Cre*$^{+/-}$ animals revealed severe dysplasia and hyperplasia in the mutant brains (Fig. 1). *αE-catenin*$^{-/-}$ventricular zone cells were dispersed throughout the developing brains, forming invasive tumor-like masses displaying widespread pseudopalisading and the formation of rosettes (Fig. 1F′), similar to Homer-Wright rosettes in human medulloblastoma, neuroblastoma, retinoblastoma, pineoblastoma, neurocytoma and pineocytoma tumors (6–8). While E12.5 *αE-catenin*$^{-/-}$ cortexes already showed some disorganization (Fig. 1B′), the general brain appearance was similar between the wildtype and *αE-catenin*$^{-/-}$ embryos (Fig. 1A–A′). In contrast, the E13.5 mutants exhibited a prominent increase in the thickness and size of the cerebral cortex (Fig. 1C–C′). Massive expansion of dysplastic cortical progenitor cells continued later in development, causing a posterior and ventral shift in localization of the lateral ventricle (Figs. 1D–E′, S3).

We next analyzed the mechanisms responsible for dysplasia in *αE-catenin*$^{-/-}$ brains. Ventricular zone progenitors are bipolar, with one extension reaching the ventricular surface and another process reaching in the opposite direction (Fig. S4A). These cells form a prominent cell-cell adhesion structure at the ventricular interface, called an apical-junctional complex. Staining with cell adhesion and cell polarity markers showed disruption of apical-junctional complexes and loss of cell polarity in *αE-catenin*$^{-/-}$ neural progenitor cells (Figs. 2, S4). Electron microscopic analyses of *αE-catenin*$^{-/-}$ brains revealed nonpolarized, round and loosely connected to each other progenitors lacking apical-junctional complexes (Fig. 2G–H). Perhaps due to residual amounts of *αN-catenin* present in the progenitor cells, small fragments of *αE-catenin*$^{-/-}$ neuroepithelium were still capable of maintaining cell polarity, but they were often engulfed by protruding nonpolarized cells, folded back on themselves and internalized to form rosettes (Figs. 2D–F, I, S4B, D). We concluded that loss of apical-junctional complexes and subsequent loss of cell polarity may represent the mechanism responsible for dysplasia in *αE-catenin*$^{-/-}$ brains.

We next analyzed the mechanisms responsible for hyperplasia in *αE-catenin*$^{-/-}$ brains. Failure of cell cycle withdrawal is responsible for hyperplasia in brains with hyperactive β-catenin pathway (9). To analyze cell cycle withdrawal in *αE-catenin*$^{-/-}$ brains, we counted the proportion of cells that had exited the cell cycle after 24h labeling with BrdU (Fig. 3B, B′). We concentrated on E13.5 mutants, since we observed the most rapid increase in total brain cell numbers during the E12.5–E13.5 interval of development. We found no significant differences in cell cycle withdrawal between the wildtype and mutant cells (Fig. 3C). To determine if differentiation was affected in *αE-catenin*$^{-/-}$ brains, we used anti-β-tubulin III and anti-nestin antibodies, neuronal and progenitor cell markers, respectively (Fig. S5A–B′). While there were no differences in appearance of E12.5 wildtype and mutant cortexes (Fig. S5A, A′), E13.5 *αE-catenin*$^{-/-}$ cortexes were disorganized and thickened with neurons present not only in the cortical plate, but also elsewhere throughout the cortex (Fig. S5B, B′). Nevertheless, the overall ratio between differentiated and nondifferentiated cells remained unchanged (Fig. S5C). Moreover, western blot analyses of total brain proteins with cell-type-specific antibodies did not reveal consistent differences between the wildtype and *αE-catenin*$^{-/-}$ brains (Fig. S5D). In addition, we found no differences between the wildtype and *αE-catenin*$^{-/-}$ brains in the position and numbers of located at the surface of cerebral cortex Cajal-Retzius neurons (Fig. S6). We concluded that despite the loss of progenitor cell polarity, the general program governing differentiation is not affected in *αE-catenin*$^{-/-}$ brains.

To analyze whether loss of αE-catenin led to changes in proliferation, we studied neural progenitor cell cycle length and number of cells in mitosis. To measure cell cycle length, we counted the proportion of neural progenitor cells labeled by a pulse of BrdU (9)(Fig. 3D–E′). We found significant shortening of the cell cycle in E13.5 *αE-catenin*$^{-/-}$ progenitor cells (Fig. 3F). In addition, E13.5 mutant brains displayed a 40% increase in the number of mitotic cells (Fig. 3G–I).

Apoptosis is also critical for regulation of total cell numbers in the developing brain (10). Counting of apoptotic cells revealed a 2-fold decrease in apoptosis in the *αE-catenin*$^{-/-}$cortexes (Fig. 3J–L). We concluded that hyperplasia in the *αE-catenin*$^{-/-}$ brains was a combined outcome of the shortening of the cell cycle and decreased apoptosis in neural progenitor cells.

To determine the molecular mechanisms responsible for hyperplasia in *αE-catenin*$^{-/-}$brains we utilized microarray approach. Surprisingly, a genome-wide analysis revealed only few changes in gene expression (Table 1), with only five transcripts upregulated and three downregulated in *αE-catenin*$^{-/-}$ brains. Interestingly, the two most upregulated cDNAs, *Fgf15* and *Gli1*, represent well known endogenous transcriptional targets of the Hh pathway (11,12). We performed quantitative reverse transcriptase PCR analysis of critical members and targets of the hedgehog pathway: *smoothened* (*Smo*), *patched1* (Ptch), *sonic hedgehog* (*Shh*), *indian hedgehog* (*Ihh*), *desert hedgehog* (*Dhh*), *Rab23*, *Gli1*, *Gli2*, *Gli3* and *Fgf15*. We found that the expression of *Gli1*, *Fgf15* and *Smo* was significantly upregulated in *αE-catenin*$^{-/-}$brains (Fig. 4A). To determine the compartment of the developing brain displaying upregulation of hedgehog signaling, we performed *in situ* hybridizations with *Gli1*, *Fgf15* and *Smo* probes (Fig. 4B–D′). We found that *Gli1* and *Fgf15* transcripts are upregulated in the progenitor cell domain of *αE-catenin*$^{-/-}$ cerebral cortex, the area most severely affected by hyperplasia in *αE-catenin*$^{-/-}$ brains (Fig. 1C′).

Upregulation of endogenous targets of the Hh signaling pathway suggests activation of this pathway in developing cortexes of the *αE-catenin*$^{loxP/loxP}$*/Nestin-Cre*$^{+/-}$ mice. While the exact mechanism responsible for αE-catenin-mediated regulation of *Gli1* and *Fgf15* is presently unknown, an increase in expression of the activator of the Hh signaling *Smo* is likely to play a causal role in abnormal activation of the Hh pathway in *αE-catenin*$^{-/-}$ brains. Indeed, *Smo* upregulation is responsible for activation of Hh signaling in cancer cell lines, and it may be a focal point of regulation of the pathway in tissue regeneration and cancer (13).

The Hh pathway plays a critical role in mammalian CNS development and brain cancer (14). Sonic hedgehog stimulates proliferation of progenitor cells in the developing cerebral cortex (15,16). In addition, Hh signaling promotes survival and blocks apoptosis of neuroepithelial cells (17). Therefore, abnormal activation of the Hh pathway may be responsible for cortical hyperplasia in *αE-catenin*$^{-/-}$ brains. To determine whether this is indeed the case, we used cyclopamine, a specific inhibitor of Smoothened (18), which can block the Hh pathway *in vivo* (19). We found that a single injection of cyclopamine at E12.5 (immediately before the onset of hyperplasia) did not interfere with depletion of αE-catenin (Fig. S7), but eliminated the differences in total cell numbers between the E13.75 wildtype and *αE-catenin*$^{-/-}$ brains (Fig. 4E). Injections of decreasing amounts of cyclopamine produced intermediate phenotypes demonstrating dose-dependence between the inhibitor and hyperplasia (Fig. S8). As expected, inhibition of Hh did not rescue cortical disorganization, which results from the disruption of adherens junctions in *αE-catenin*$^{-/-}$ brains (Fig. S9). Analyses of the cell cycle length and apoptosis showed rescue of the cell cycle and apoptosis abnormalities in cyclopamine-treated *αE-catenin*$^{-/-}$ brains (Figs. 4E, S9C-H′). As expected, cyclopamine injection led to a significant decrease in expression of the Hh pathway transcriptional targets *Gli1* and *Fgf15* (Fig. S10). We concluded that abnormal activation of the Hh pathway was responsible for

shortening of the cell cycle, decreased apoptosis and subsequent hyperplasia in *αE-catenin*$^{-/-}$ cerebral cortexes.

Our findings allow us to propose a model of a negative feedback loop regulating the rates of cell proliferation to control the size of the cerebral cortex (Fig. S11). In this "crowd control" model, the increase in cell density, which is sensed by an increase in the per cell area occupied by adherens junctions (Fig. S11A), is translated into downregulation of Hh signaling and subsequent decrease in cell proliferation (Fig. S11B). The abnormal decrease in cell density, which is measured by destabilization and paucity of adherens junctions, is translated into activation of Hh pathway and subsequent acceleration of cell proliferation, until the normal cell density is achieved. Therefore, the density of cellular crowd ultimately regulates the rates of cell accumulation during normal development. Solid tumors may escape "crowd control" of cell proliferation by destabilizing the adherens junctions, one of the frequent events reported in human cancers (20).

Supplementary Material

Refer to Web version on PubMed Central for supplementary material.

Acknowledgements

We thank Drs. Philippe Soriano, Susan Parkhurst, Stephen Tapscott, Daniel Gottschling and Bruce Edgar and all members of Dr. Vasioukhin's laboratory for advice and encouragement, Drs. Nagafuchi, Tsukita and Developmental Studies Hybridoma Bank for generous gift of antibodies. Linda Cherepoff, Franque Remington, Manda Null and Brad Helbing for help with histology, electron microscopy, genotyping and manuscript preparation, respectively. This work was supported by the NCI grant R01 CA098161.

References

1. Chenn A, Zhang YA, Chang BT, McConnell SK. Mol Cell Neurosci Jul;1998 11:183. [PubMed: 9675050]
2. Hirano S, Kimoto N, Shimoyama Y, Hirohashi S, Takeichi M. Cell Jul 24;1992 70:293. [PubMed: 1638632]
3. Vasioukhin V, Bauer C, Yin M, Fuchs E. Cell Jan 21;2000 100:209. [PubMed: 10660044]
4. Vasioukhin V, Bauer C, Degenstein L, Wise B, Fuchs E. Cell Feb 23;2001 104:605. [PubMed: 11239416]
5. Graus-Porta D, et al. Neuron Aug 16;2001 31:367. [PubMed: 11516395]
6. Sangueza OP, Sangueza P, Valda LR, Meshul CK, Requena L. J Am Acad Dermatol Aug;1994 31:356. [PubMed: 8034805]
7. Graham, DI.; Lantos, PL. Greenfield's Neuropathology. Arnold; New York, NY: 2002.
8. Burger, PC.; Scheithauer. Tumors of the central nervous system. Armed Forces Institute of Pathology; Washington, DC: 1994. Atlas of tumor pathology.
9. Chenn A, Walsh CA. Science Jul 19;2002 297:365. [PubMed: 12130776]
10. Depaepe V, et al. Nature Jun 30;2005 435:1244. [PubMed: 15902206]
11. Ishibashi M, McMahon AP. Development Oct;2002 129:4807. [PubMed: 12361972]
12. Saitsu H, et al. Dev Dyn Feb;2005 232:282. [PubMed: 15614767]
13. Karhadkar SS, et al. Nature Oct 7;2004 431:707. [PubMed: 15361885]
14. Ruiz IAA, Palma V, Dahmane N. Nat Rev Neurosci Jan;2002 3:24. [PubMed: 11823802]
15. Dahmane N, et al. Development Dec;2001 128:5201. [PubMed: 11748155]
16. Palma V, Ruiz i Altaba A. Development Jan;2004 131:337. [PubMed: 14681189]
17. Thibert C, et al. Science Aug 8;2003 301:843. [PubMed: 12907805]
18. Chen JK, Taipale J, Cooper MK, Beachy PA. Genes Dev Nov 1;2002 16:2743. [PubMed: 12414725]
19. Berman DM, et al. Science Aug 30;2002 297:1559. [PubMed: 12202832]

20. Cavallaro U, Christofori G. Nat Rev Cancer Feb;2004 4:118. [PubMed: 14964308]

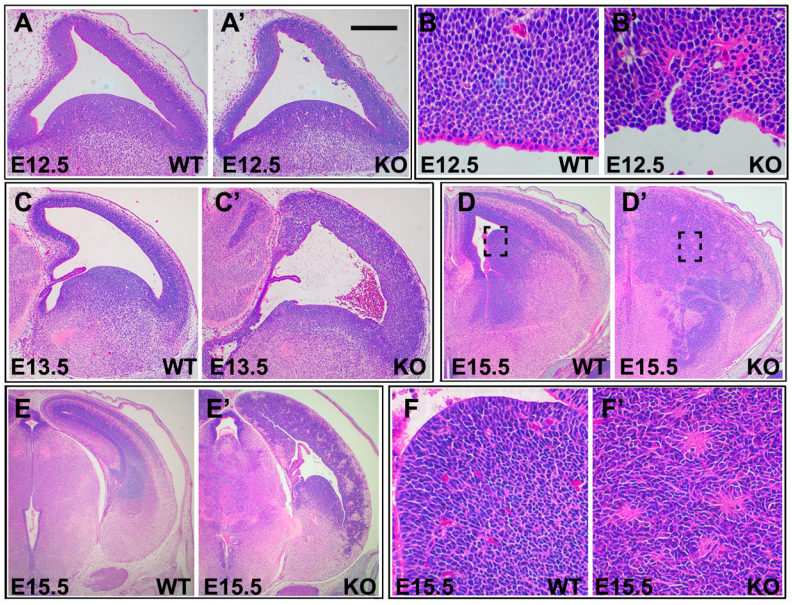

Fig. 1.

Severe dysplasia and hyperplasia in *αE-catenin*$^{-/-}$ brain. Histologic appearance of brains from wildtype (WT) and *αE-catenin*$^{LoxP/LoxP}$*/Nestin-Cre*$^{+/-}$ (KO) mice. Sagittal sections through developing telencephalon from the wildtype (A, C) and *αE-catenin*$^{-/-}$ (A′, C′) brains of E12.5 (A, A′) and E13.5 (C, C′) embryos. Ventricular zone of the cerebral cortex from the E12.5 wildtype (B) and *αE-catenin*$^{-/-}$ (B′) brains. Coronal sections from the E15.5 wildtype (D, E, F) and *αE-catenin*$^{-/-}$ (D′, E′, F′) brains. Areas in dashed squares in D, D′ are shown at higher magnification in F, F′. Bar in A′ represents 0.27 mm in A, A′; 0.36 mm in C–C′; 0.42 mm in D, D′; 0.54 mm in E–E′; 50 km in F, F′, 40 km in B, B′.

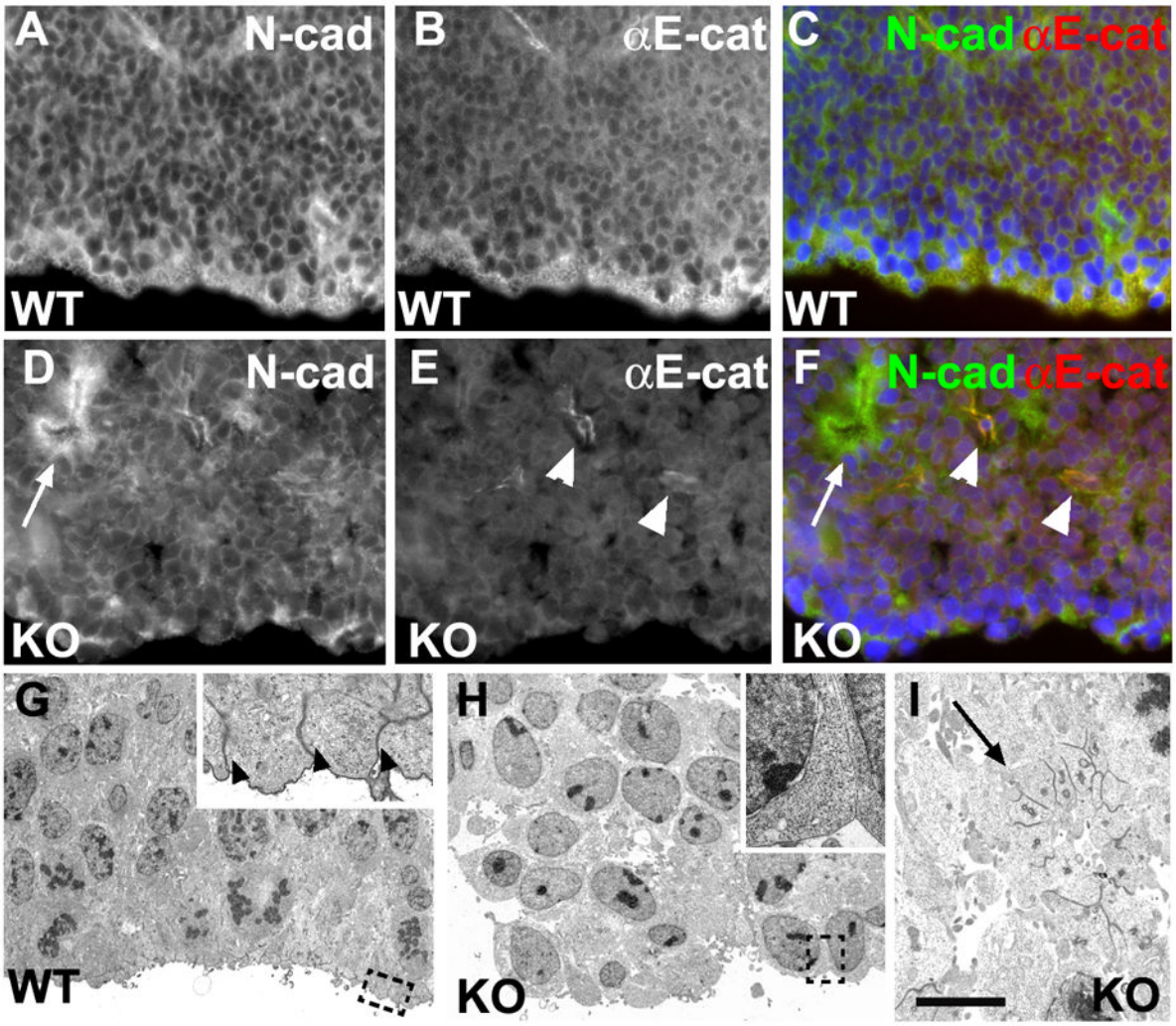

Fig. 2.

Loss of cell polarity and disruption of apical-junctional complex in *αE-catenin*$^{-/-}$neural progenitor cells. **(A–F)** Disruption of apical adherens junctions in *αE-catenin*$^{-/-}$ neural progenitors. Staining with anti-N-cadherin (A, D; green in C, F) and anti-αE-catenin (B, E; red in C, F) antibodies. **(G–I)** Electron microscopy analysis of cortical neural progenitor cells of E12.5 wildtype (G) and *αE-catenin*$^{-/-}$ (H, I) embryos. Areas in dashed squares in G, H are magnified in insets. Arrowheads in inset to G denote missing in mutants apical-junctional complexes. Arrows indicate internalization of polarized neuroepithelium and formation of rosette-like structures maintaining apical-junctional complexes. Arrowheads in E, F denote blood vessels not targeted by Nestin-Cre. Bar in I corresponds to 30 km in A–F; 10 km in G–H, 4 km in I and 1.8 km in insets to G–H.

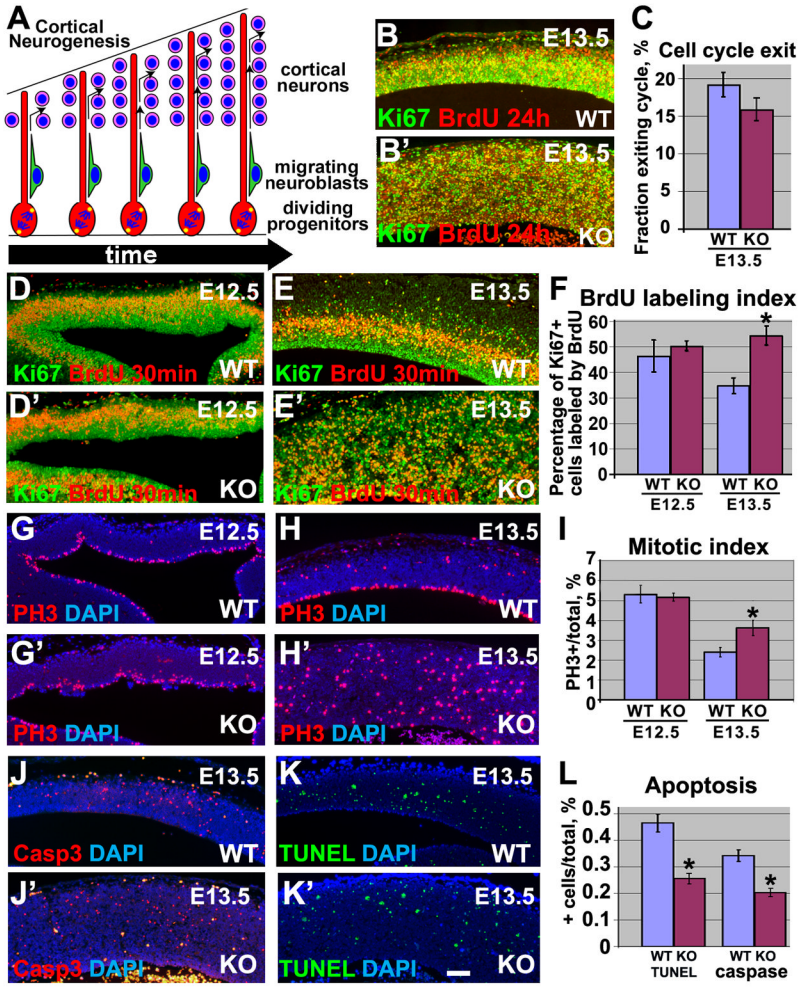

Fig. 3.

Shortening of cell cycle and decreased apoptosis in *αE-catenin*$^{-/-}$ cerebral cortexes. **(A)** Model of cortical neurogenesis. **(B, B′)** Minor changes in cell cycle withdrawal in *αE-catenin*$^{-/-}$ cortexes. Pregnant females were injected with BrdU 24h before being sacrificed. Cells re-entering cell cycle are BrdU^{+}/Ki67^{+}, while cells withdrawn from cell cycle are BrdU^{+}/Ki67^{-}. **(C)** Quantitation of experiments shown in B-B′. Cell cycle exit is determined as a ratio of cells exited cell cycle (BrdU^{+}/Ki67^{-}) to all cells incorporated BrdU. n=3. **(D–E′)** Decrease in cell cycle length in *αE-catenin*$^{-/-}$ progenitors. Higher percentage of *αE-catenin*$^{-/-}$progenitor cells (Ki67^{+}) are labeled with BrdU after 30 min pulse. **(F)** Quantitation of experiments shown in D–E′. BrdU labeling index is a percentage of Ki67^{+} cells incorporated BrdU. n=3. *P<0.001. **(G–H′)** Immunostaining of cortical sections from wildtype and *αE-catenin*$^{-/-}$ brains with anti-phospho-histone 3 (red) antibodies reveals increase in mitotic cells in E13.5 mutants. DNA was counterstained by DAPI (blue). **(I)** Quantitation of the experiments shown in G–H′. Mitotic index is a ratio of mitotic cells to the total brain cell number. n=3. *P<0.001. **(J–K′)** Decrease in apoptosis in *αE-catenin*$^{-/-}$ cortexes. Apoptotic cells in the wildtype (J–K) and mutant (J′–K′) brains were detected by staining with anti-cleaved caspase 3 (Casp3) and TUNEL stainings. **(L)** Quantitation of experiments shown in J–K′. Ratios of Casp3^{+} or TUNEL^{+} cells per total cell numbers are shown. n=3. *P<0.001. Bar in frame K′ represents 100 km for B–B′, D–K′.

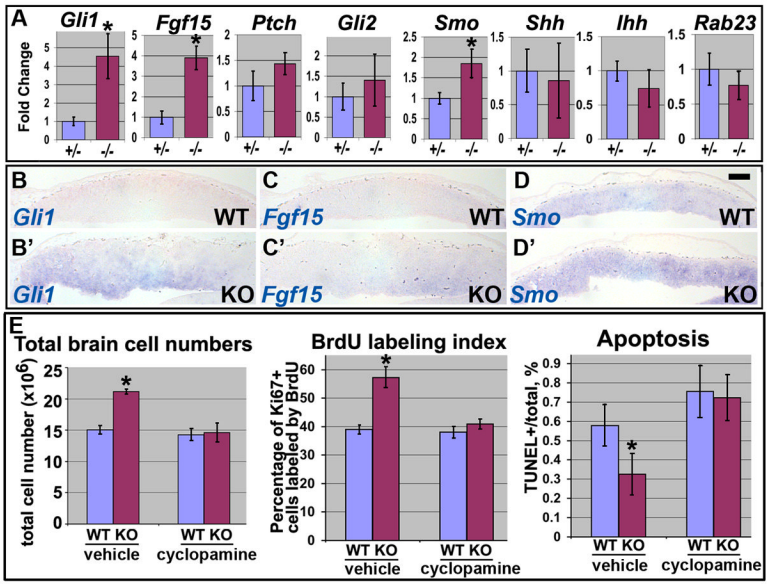

Fig. 4.

Activation of Hh pathway is responsible for shortening of cell cycle, decreased apoptosis and subsequent hyperplasia in *αE-catenin*$^{-/-}$ cerebral cortexes. **(A)** qPCR analysis of Hh pathway transcripts in E12.5 heterozygous and mutant brains. The levels of expression are shown in arbitrary units with mean heterozygous levels adjusted to one. Data represent means ± SD. N≥4. *P<0.002. **(B–D′)** Cortical sections from E12.5 wildtype and αE-catenin$^{-/-}$embryos were analyzed by *in situ* hybridization with *Gli1*, *Fgf15* and *Smo* probes. Bar in frame D represents 200km. **(E)** Inhibition of Hh pathway by cyclopamine eliminates thedifferences in total cell numbers, cell cycle length and apoptosis between the wildtype and *αE-catenin*$^{-/-}$ brains. Pregnant females were injected with 10mg/kg of cyclopamine in 2-hydropropyl-β-cyclodextrin (vehicle) or vehicle alone at E12.5 and embryos were analyzed 30h later. Quantitation was performed as described in Figs. 3, S2. Data represent means ± SD. N≥3. *P<0.001.

Table 1

Differentially expressed genes in E12.5 αE-catenin$^{-/-}$ brains

RNAs from *αE-catenin$^{LoxP/+}$/Nestin-Cre$^{+/-}$* and *αE-catenin$^{LoxP/LoxP}$/Nestin-Cre$^{+/-}$* brains were analyzed by Affymetrix expression arrays. Relative fold change is calculated with respect to heterozygous brains. Bayes.p is the p-value obtained using the CyberT Bayesian statistical framework.

Name	Symbol	UGCluster	Relative fold change	Bayes.p
Upregulated				
fibroblast growth factor 15	Fgf15	Mm.3904	2.39	1.31E-06
GLI-Kruppel family member GLI	Gli1	Mm.336839	2.37	3.34E-06
RIKEN cDNA A830059I20 gene	A830059I20Rik	Mm.113787	1.98	5.86E-07
expressed sequence AU040576	AU040576	Mm.26700	1.93	2.27E-05
high mobility group AT-hook 1	Hmga1	Mm.4438	1.59	1.60E-05
Downregulated				
p53 binding protein 1	Trp53bp1	Mm.215389	−3.91	6.70E-06
RIKEN cDNA 2900097C17 gene	2900097C17Rik	Mm.349235	−2.63	5.41E-06
RIKEN cDNA A730017C20 gene	A730017C20Rik	Mm.209711	−1.92	2.55E-07